Colloids confined to a flexible container

Lutz Maibaum, Matthias Schmidt, Hartmut Löwen

Institut für Theoretische Physik II, Heinrich-Heine-Universität Düsseldorf, Universitätsstraße 1, D-40225 Düsseldorf, Germany

A model of hard spheres trapped inside a container of fluctuating shape is proposed to describe colloidal particles in a vesicle or in an emulsion droplet. The container is assumed to be the convex hull of the particles and is described by an integral geometric approach including volume and surface terms. In the limit of large volume coupling, the model reduces to the well-known geometric problem of natural bin packing. Using computer simulations and cell theory, we calculate equilibrium properties for various finite numbers of confined particles in conformations ranging from clusters to planar and linear structures and identify transitions between these different conformations.

I. INTRODUCTION

Clusters are present in a variety of systems, ranging from atomic systems [1] such as silicon [2] or noble gases [3] to aggregated colloidal suspensions. Clusters are built up by a finite number of particles that tend to be closely separated. The structural organization inside a cluster can be very rich and originates from the interactions between particles and the interaction with the surrounding. One simple mechanism to generate such structures is the packing of hard spheres (HS) under different boundary conditions.

The efficient packing of spheres is an old problem dating back to Kepler and Gauss [4]. One question concerns the densest packing of an infinite number of spheres. Only recently, a mathematical proof stating that no packing denser than a face-centered-cubic structure (fcc) is possible in three dimensions was announced and published in parts [5]. Related problems are optimal shapes of compact strings [6] and the efficient packing of a finite number of spheres inside a given container. A particular simple container is the *natural bin*. This is the smallest convex body that contains a given configuration of spheres. It is canonical to ask for the configuration of spheres that leads to the smallest natural bin. Contrary to intuition, this is not a spherelike cluster for a small number of spheres. Up to 56 spheres, a linear configuration in which the sphere centers lie on a straight line (''sausage'') is denser than any spherelike or platelike configuration. In four dimensions, the crossover from a sausage to a spherelike cluster happens at about 300 000 spheres. This effect has become known as the ''sausage catastrophe'' [4,7].

Hard spheres are widely used to model dense liquids and solids and they can be experimentally realized by suspensions of sterically stabilized *PMMA* particles [8,9]. Besides the bulk freezing transition into an fcc crystal, hard spheres have been considered in a variety of confining situations, such as confinement between parallel plates [10,11], inside a spherical cavity [12–14], or inside emulsion droplets [15]. In all these cases, there is rigid confinement: The pores do not change their shapes.

However, shape fluctuations do exist in nature. Examples are the deformations of liquid droplets in emulsions, where the surface tension between the continuous phase, say water, and the dispersed phase, say oil, tends to keep the droplet shape spherical and thermal fluctuations tend to deform this ideal shape. Another system that exhibits many complicated shapes is vesicles [16,17], which are closed two-dimensional membranes [18] that are suspended in a molecular liquid. Besides the fluctuations of a spherical object, toroidal configurations with holes or even starlike shapes are possible. They originate from the highly nontrivial membrane structure itself, including curvature and elasticity contributions.

Colloidal particles can be trapped inside larger objects in quite a number of ways. Experimentally realized examples are magnetic beads inside biological cells [19], liquid droplets inside liquid droplets in double emulsions [20], small vesicles inside giant ones [21], and colloidal particles inside lipid bilayer vesicles [22]. Vesicles in contact with nanoparticles and colloids were studied also theoretically [23].

In the present work, we investigate which shape fluctuations can be driven not by the membrane itself but by colloidal particles that are imprisoned inside the object. The shape fluctuations are coupled to the positions of the colloidal particles resulting in new cluster structures as well as new vesicle shapes. One interesting question is whether the peculiar transition from a compact cluster to a linear configuration, the sausage catastrophe, is present in a system that not only describes close-packed structures, but also accounts for the entropy due to the positional degrees of freedom of the particles. We consider particles inside a container, which is modeled through a coarse-grained approach involving an integral geometric description. Integral geometry is a powerful tool that is becoming increasingly popular [24]. There are applications ranging from microemulsions [25] to complex fluids [26,27]. The basic ingredients of our model involve a surface tension and an external pressure acting on the container modeled as surface and volume couplings. As a result, we identify different types of conformations corresponding to rodlike, platelike, and spherelike vesicle shapes, and we determine their relative stability as a function of temperature by using cell theory and computer simulations.

The paper is organized as follows. In Sec. II, we define our theoretical model for colloids inside a fluctuating object. A cell theory is developed in Sec. III. Details of the Monte Carlo computer simulation are given in Sec. IV. Results

thereof are presented in Sec. V, and compared to cell theory. We finish with concluding remarks in Sec. VI.

II. MODEL OF COLLOIDS IN A CONTAINER

A. Definition of the model

We consider N hard spheres with diameter σ with position coordinates $\mathbf{r}_i$, $i=1,...,N$ in three spatial dimensions that interact with the pair potential,

$$\phi(r) = \begin{cases} \infty & \text{if } r < \sigma \\ 0 & \text{otherwise,} \end{cases}$$

where r is the separation distance between two particles. The number of particles we consider is finite and small, typically $N=2-55$.

The particles are wrapped into a closed membrane that is modeled as the convex hull of the set of spheres $\{\mathbf{r}_i\}$. Mathematically, the convex hull of one or more geometric bodies is the smallest convex body that encloses the basic objects. A body is called convex if for any two points inside the body all points that lie on a straight line between both points lie also inside the body. The convex hull is a uniquely defined object.

The physical motivation for using the convex hull is a situation in which the surface tension between the inside and the outside is large enough so that any free deformation of the membrane can be neglected. On the other side, the thermal energy $k_B T$ of the colloids is large enough, so that they can move and squeeze the membrane. To allow for volume growth, oil may diffuse into the inside of the vesicle.

Once we have established the membrane shape, it is straightforward to assign a potential energy ϕ_{Hull} to it by considering integral geometry,

$$\phi_{\text{Hull}} = J_V V + J_A A + J_M M + J_\chi \chi. \tag{1}$$

Here, the Minkowski functionals or Quermass integrals (see, e.g., Ref. [25]) are volume V, surface area A, integral of mean curvature M, and the Euler characteristic χ of the convex hull. For a convex body $\chi = 4\pi$ holds, so J_χ is an irrelevant parameter for the current investigation and is set to zero without loss of generality. A nonzero value of J_χ may be of interest once fission processes of the container are taken into account, or, e.g., toroidal shapes are considered. Furthermore, we set the coupling to the mean curvature to zero, $J_M = 0$. This ensures that the model does not favor spontaneous curvature. The remaining coupling constants are volume coupling, J_V, modeling an external pressure acting on the container, and a surface tension J_A. We define dimensionless parameters as $\lambda_V = J_V \sigma^3/(k_B T)$ and $\lambda_A = J_A \sigma^2/(k_B T)$. See Fig. 1 for a sketch of the model.

B. Computational details

Let us show how the container volume and surface area can be computed efficiently. We exploit the relation of the convex hull of a set of spheres and the convex hull of the corresponding sphere centers. In both cases the crucial point is to identify which points (or spheres) contribute to the hull,
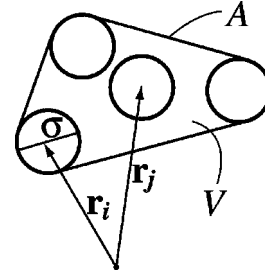

FIG. 1. Sketch of the model of colloids inside a container. The circles represent the particles with diameter σ; $\mathbf{r}_i$ and $\mathbf{r}_i$ are position vectors. The solid line is the convex hull with surface S and volume V. The model considered in this work is three-dimensional.

i.e., lie at the boundary, and which of the points lie inside and do not contribute to the hull. For a collection of points this is a well-known problem in geometry and efficient numerical algorithms are available [28]. We start from the set $\mathbf{r}_i$ and identify the boundary points, denoted by $\mathbf{r}_j^{(0)}$. The $\mathbf{r}_j^{(0)}$ define the corners of a polyhedron, which we call the *core* of the container. Elementary geometry is used to calculate the Minkowski functionals V_0, A_0, M_0 of the core. In particular, the core surface is obtained by summing up the surface areas of all its faces. The integral mean curvature is

$$M_0 = \frac{1}{2} \sum_k l_k \alpha_k, \tag{2}$$

where l_k is the length of ridge k and α_k is the angle between the normal vectors of the two faces adjacent to ridge k. As the actual container is the parallel body of radius R to the container core, we can use Steiner's theorem (see, e.g., Ref. [25]) to obtain

$$V = V_0 + A_0 R + M_0 R^2 + 4\pi R^3/3, \tag{3}$$

$$A = A_0 + 2M_0 R + 4\pi R^2, \tag{4}$$

$$M = M_0 + 4\pi R. \tag{5}$$

C. Relation to the Helfrich Hamiltonian

Concerning the status of the model ϕ_{Hull} introduced above, we note that the familiar Helfrich Hamiltonian [29,17] for membranes is recovered if the membrane conformations are restricted to convex hulls of spheres. To see this, consider

$$\phi_{\text{Helfrich}} = \oint dA \left[\frac{\kappa}{2} \left(\frac{1}{r_1} + \frac{1}{r_2} - \frac{1}{r_s} \right)^2 + \frac{\bar{\kappa}}{r_1 r_2} \right], \tag{6}$$

where r_S is the radius of spontaneous curvature, κ is the bending rigidity, $\bar{\kappa}$ is the elastic modulus of Gaussian curvature, and the local curvature radii on the surface are denoted by r_1 and r_2. If the set of possible surface shapes is restricted to convex hulls of N spheres of radius R, we obtain

$$\phi_{\text{Helfrich}} = \frac{\kappa}{2 r_S^2} A + \left(\frac{\kappa}{R} - \frac{2\kappa}{r_S} \right) \mathcal{M} + (\kappa + \bar{\kappa}) \chi, \tag{7}$$

which is a linear combination of Minkowski functionals, apart from the missing volume term precisely like the container energy ϕ_{Hull}. The parameters are related by $J_{\mathcal{A}} = \kappa/(2r_S^2)$, $J_{\mathcal{M}} = (\kappa/R) - (2\kappa/r_S)$, and $J_{\chi} = \kappa + \bar{\kappa}$.

D. Ensembles

The central quantity in the microcanonical ensemble is the density of states, defined as

$$\Omega(V',A') = \int d\mathbf{r}_1 \cdots \int d\mathbf{r}_N$$
$$\times \delta[V' - V(\{\mathbf{r}_i\})] \delta[A' - A(\{\mathbf{r}_i\})], \quad (8)$$

where the integration only runs over allowed hard-sphere configurations. The (microcanonical) entropy is obtained as $S = k_B \ln \Omega$. The central quantity in the canonical ensemble is the partition sum

$$Z = \frac{1}{\Lambda^{3N} N!} \int d\mathbf{r}_1 \cdots \int d\mathbf{r}_N e^{-\beta \phi(\mathbf{r}_1, \ldots, \mathbf{r}_N)}, \quad (9)$$

where Λ is the thermal wavelength of the colloids. The Helmholtz free energy is $F = -k_B T \ln Z$. Note that as we are dealing with a finite system, the canonical and the microcanonical ensembles are not equivalent.

III. CELL THEORY

The cell theory (CT) is a simple, yet accurate, approach to hard-sphere systems. Crystals are well-described in bulk [30,31] as well as in rigid confined geometries [10,11] and near walls [32]. Here we generalize the concept to flexible confinement. The striking feature of yielding an exact upper bound to the free energy is preserved.

A. General scheme

Our strategy consists of two steps. First, we constrain the colloids to fixed cells in space. Instead of integrating over all space, we require the center of each particle i to lie inside its cell C_i. Thus, the integration region in the partition sum [Eq. (9)] becomes smaller. Second, we construct a body K^* that is larger than any possible container K in this restricted system. Replacing the volume and the surface in the Boltzmann factor by those of K^*, the Boltzmann factor also becomes smaller and the approximate partition sum Z^* we obtain is a lower bound to the exact partition sum Z. From that naturally an upper bound to the free energy is obtained.

In detail we proceed as follows. Let us introduce the notion of cells C_i, $i = 1, \ldots, N$, which are geometric objects that are constructed such that they have a distance of at least the particle diameter σ from each other. If each particle i is confined to its cell C_i, the particles of neighboring cells cannot overlap. We can then drop the hard-core term in the Boltzmann factor and obtain

$$Z \geqslant \frac{1}{\Lambda^{3N}} \int_{C^{(1)}} d\mathbf{r}_1 \cdots \int_{C^{(N)}} d\mathbf{r}_N \exp[-\beta \phi_{\text{Hull}}(\{\mathbf{r}_i\})] \quad (10)$$

$$= \frac{1}{\Lambda^{3N}} \int_{C^{(1)}} d\mathbf{r}_1 \cdots \int_{C^{(N)}} d\mathbf{r}_N \exp[-\lambda_V V(\{\mathbf{r}_i\})$$
$$- \lambda_A A(\{\mathbf{r}_i\})], \quad (11)$$

where the factor $1/N!$ in the definition of Z, Eq. (9), is canceled by the number of possibilities to distribute N particles on N cells.

In order to obtain a tractable integral, we construct an approximate container

$$K^* = \bigcup_{\mathbf{r}_i \in C_i} K(\{\mathbf{r}_i\}), \quad (12)$$

which is the union of all possible K that are realized if each particle moves freely inside its cell. The crucial point is that K^* is independent of the position coordinates $\mathbf{r}_i$. This will allow us to carry out the integrations over space, Eq. (11). K^* depends, however, on the shape and positions of the C_i. In particular, it can be computed as the parallel body of radius R of the convex hull ($\mathcal{C}$, see also Sec. II A) of the cells,

$$K^* = \Gamma_R, \quad (13)$$

$$\Gamma = \mathcal{C}(C_1, \ldots, C_N), \quad (14)$$

where the subscript denotes the parallel body with radius R. If Γ is known, Steiner's theorem can be used to calculate the volume V^* and surface area A^* of K^*. Due to the definition of K^* and the fact that only convex bodies are involved,

$$V^* \geqslant V(\{\mathbf{r}_i \in C_i\}), \quad (15)$$

$$A^* \geqslant A(\{\mathbf{r}_i \in C_i\}) \quad (16)$$

hold. Finally, the lower bound $Z^* < Z$ for the partition function is obtained as

$$Z^* = \frac{1}{\Lambda^{3N}} \int_{C^{(1)}} d\mathbf{r}_1 \cdots \int_{C^{(N)}} d\mathbf{r}_N e^{-\lambda_V V^* - \lambda_A A^*} \quad (17)$$

$$= \exp(-\lambda_V V^* - \lambda_A A^*) \prod_{i=1}^{N} [v_{\text{free}}^{(i)}/\Lambda^3] \quad (18)$$

$$= \exp(-\lambda_V V^* - \lambda_A A^*)(v_{\text{free}}/\Lambda^3)^N, \quad (19)$$

where $v_{\text{free}}^{(i)}$ is the volume of cell C_i. The last equality holds if all cells have the same volume $v_{\text{free}} = v_{\text{free}}^{(i)}$. The free energy within CT is readily obtained as

$$F^* = -k_B T \ln Z^* \quad (20)$$

$$= -N k_B T \ln(v_{\text{free}}/\Lambda^3) + k_B T(\lambda_V V^* + \lambda_A A^*), \quad (21)$$

where the property of being an upper bound $F^* > F$ to the exact free energy is inherited from the bound to the partition
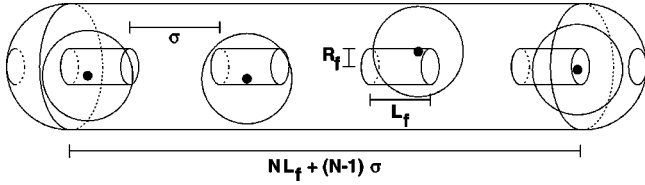
FIG. 2. Cell model for sausage configurations. Shown are particles (spheres), cells (cylinders), and the container K^* (enclosing cigarlike shape).

sum. The remaining task is to optimize with respect to the positions of the cells in space, their shape, and their size. Then V^* and A^* serve as estimates for average container volume and average surface area.

B. Application to different structures

The structure of the (crystalline) arrangement of particles is an input to the CT. We prescribe this by specifying the positions c_i of the cell centers. All cells are chosen to have an identical shape C. Calculation of the body Γ [Eq. (14)] yields volume V^* and surface area A^* of the approximate container K^*. In the following, this recipe is carried out for the three types of conformations under consideration, see also Fig. 3.

1. Rodlike shapes (''sausages'')

We assume a one-dimensional arrangement of cells, $\mathbf{c}_i = id\mathbf{e}$, where the cells are labeled by $i=1,...,N$, d is the distance between cell centers, and $\mathbf{e}$ is some unit vector that we refer to as ''sausage axis.'' The free volume for each particle is assumed to be rotationally symmetric around $\mathbf{e}$, and to have different magnitudes along and perpendicular to $\mathbf{e}$. Hence the cell is a cylinder with radius r_f and height l_f, and is aligned along $\mathbf{e}$. The distance between the centers of two neighboring cells must be $d=\sigma+l_f$, so overlap of neighboring particles cannot occur. Obviously the convex hull Γ of the cells is a cylinder of length $Nl_f+(N-1)\sigma$ and radius r_f. Its Minkowski functionals are

$$V_\Gamma = \pi r_f^2 [Nl_f+(N-1)\sigma], \qquad (22)$$

$$A_\Gamma = 2\pi r_f [Nl_f+(N-1)\sigma]+2\pi r_f^2, \qquad (23)$$

$$M_\Gamma = \pi^2 r_f + \pi[Nl_f+(N-1)\sigma]. \qquad (24)$$

The volume V^* and surface area A^* of the approximate container K^*, see Fig. 2, are obtained through Steiner's theorem as

$$V^* = \pi \left[Nl_f r_f^2 + (Nr_f^2+Nl_f r_f)\sigma + \left(N-1+\frac{\pi}{4}\right)r_f\sigma^2 \right.$$

$$\left. + \frac{Nl_f\sigma^2}{4} + \left(\frac{N-1}{4}+\frac{\pi}{6}\right)\sigma^3 \right], \qquad (25)$$

$$A^* = \pi[2r_f^2 + 2Nl_f r_f + (2N-2+\pi)r_f\sigma \qquad (26)$$

$$+ Nl_f\sigma + (N-1+\pi)\sigma^2]. \qquad (27)$$

F^* can be easily minimized numerically with respect to l_f and r_f.

2. Platelike shapes (''Pizzas'')

The cell centers are assumed to build a portion of a two-dimensional (2D) hexagonal lattice with lattice spacing d. Hence $\mathbf{c}_i = jd\mathbf{e}_1 + (\sqrt{3}/2)kd\mathbf{e}_2$, where j, k are integers enumerating lattice sites, and the $\mathbf{e}_i$ build the basis of the Cartesian coordinate system. The cells are assumed to be different in magnitude within the $\mathbf{e}_1-\mathbf{e}_2$ ''pizza plane'' and perpendicular to it. For simplicity, we assume rotationally symmetric cells around $\mathbf{e}_3$. Hexagonal shapes could be considered, but we expect the differences to be small [33]. Hence C again is a cylinder with radius r_f and height l_f, and is aligned along $\mathbf{e}_3$. In order to avoid overlap, $d=\sigma+2r_f$.

We obtain with straightforward calculus

$$V_\Gamma = \mathcal{A}''l_f, \qquad (28)$$

$$A_\Gamma = 2\mathcal{A}'' + \mathcal{U}''l_f, \qquad (29)$$

$$M_\Gamma = \frac{\pi}{2}\mathcal{U}'' + \pi l_f, \qquad (30)$$

where

$$\mathcal{A}'' = \gamma^2 \mathcal{A}' + \gamma \mathcal{U}' r_f + 4\pi r_f^2, \qquad (31)$$

$$\mathcal{U}'' = \gamma \mathcal{U}' + 2\pi r_f, \qquad (32)$$

and A' and U' are the surface area and perimeter of the hull of the cell positions $\mathbf{c}_i$. The precise arrangement of cells only enters through A' and U'. This remarkable property is even true for arbitrary 2D cell arrangements other than portions of the hexagonal lattice.

3. Spherelike shapes (''clusters'')

In contrast to the above structures, clusters are (approximately) isotropic in all three spatial directions. Therefore, we choose spherical cells of radius r_f.

From V', A', M' of the hull of the $\mathbf{c}_i$, the body K^* can be computed as the parallel body with radius $R+r_f$. Volume V^* and surface A^* are directly obtained without the need to calculate Γ as

$$V^* = V' + A'(R+r_f) + M'(R+r_f)^2 + \frac{4\pi}{3}(R+r_f)^3, \qquad (33)$$

$$A^* = A' + 2M'(R+r_f) + 4\pi(R+r_f)^2. \qquad (34)$$

IV. COMPUTER SIMULATION

We have performed Monte Carlo (MC) simulations for particle numbers $N=4,13,55$. These were done in the canonical ensemble with prescribed (reduced) volume and surface coupling. Each MC consists of a check for possible overlap with other particles, as well as calculation of the change in the hull potential energy ϕ_{Hull}. For $N>4$, the
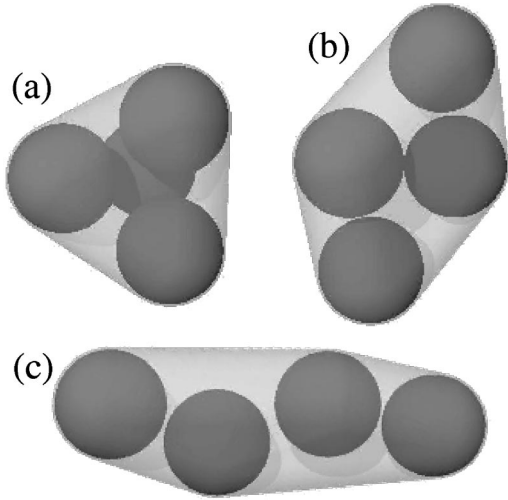
FIG. 3. Different conformations. (a) Spherelike (cluster), (b) platelike (pizza), (c) rodlike (sausage).

quick hull algorithm [28] is used to identify the convex hull of the position coordinates. Using umbrella sampling, we obtain the microcanonical entropy as a function of volume and surface. This is a delicate task that we only do for small $N=4$. Typically, between 10^7 ($N=4$) and 5×10^5 ($N=55$) MC moves per particle were done.

V. RESULTS

A. Entropy landscape

As an illustration, let us first show snapshots of typical configurations including cluster, sausage, and pizza in Fig. 3. For $N=4$, we have calculated the complete entropy landscape as a function of volume V and surface area A (see Fig. 4). There are three maxima in the entropy, which are indicated by the dark color. These are separated by ''forbidden regions'' (white), which do not contain any allowed configurations. The gap between the sausage and the pizza state is considerably bigger than the gap between the pizza and the
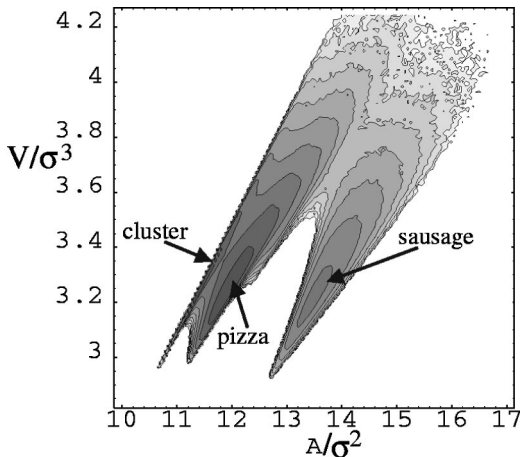

FIG. 4. Contour plot of the entropy $S(V,A)-\lambda_V V$ with $\lambda_V = 15$ as a function of the container volume V and surface area A for $N=4$.
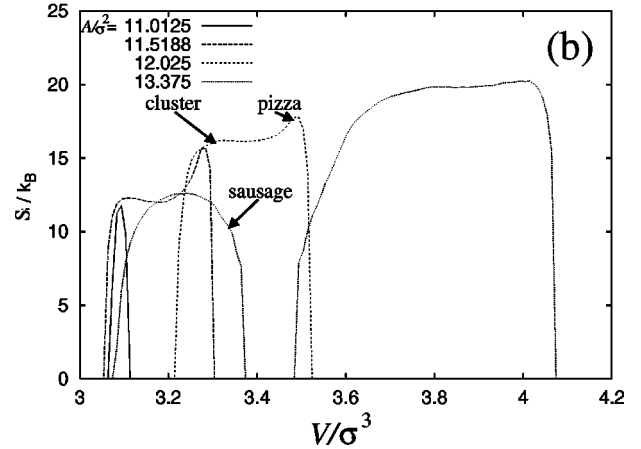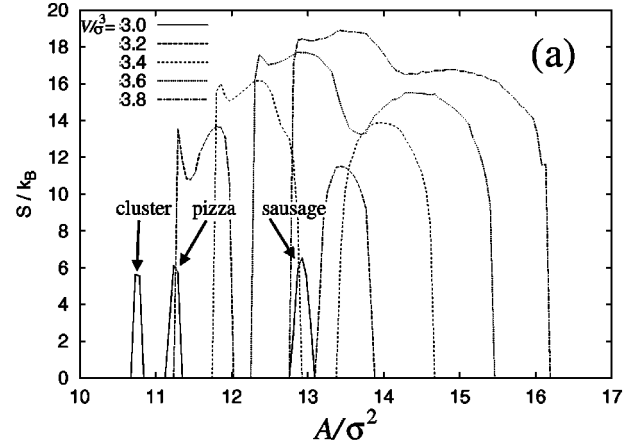

FIG. 5. One-dimensional cuts of the entropy landscape. (a) S/k_B at fixed values of volume V/σ^3 (as indicated) as a function of surface area A/σ^2. (b) S/k_B at fixed values of A/σ^2 (as indicated) as a function of V/σ^3.

cluster states. Figure 5(a) shows intersections of the entropy landscape with lines of constant volume. One observes that for V fixed to $3\sigma^3$, there are three separate regions of finite entropy, representing the three classes of configurations. For this fixed volume, it is thus not possible to switch continuously from one class to the other. For $V=3.2\sigma^3$, on the other hand, there is a connection between the cluster and the pizza region, while the sausage configurations still appear in a separate peak. Only for $V\geq3.6\sigma^3$ is there a continuous connection between all these states. In Fig. 5(b), intersections with lines of constant surface area are shown. For $A=11.0125\sigma^2$, only the cluster state has a finite entropy. For intermediate values $A=11.5188\sigma^2,12.025\sigma^2$ the pizza also appears and is separated by a pronounced minimum from the cluster. For $A=13.375\sigma^2$, this minimum becomes shallower and shifts towards larger V. An additional maximum appears for small V due to the sausage conformations.

B. Canonical averages

For large N, it becomes increasingly hard to perform a sampling of the complete configuration space using simulations. The computation of the container properties slows

down the speed of the simulation. In addition, for many particles the system has a large number of stable and metastable states, making the sampling with correct statistical weights much more difficult.

However, it is possible to study specific structures of the system. This is similar to the treatment in CT. We will compare results from CT and MC for systems with small ($N=4$), medium ($N=13$), and large ($N=55$) particle numbers. Remember that $N=55$ is a boundary case, where the sausage is still denser than any cluster.

We compute canonical averages $\langle V \rangle$ and $\langle A \rangle$, for volume and surface area, respectively, as a function of the coupling parameter λ_V. See Fig. 6(a) for a comparison of simulation and cell theory for $N=4$. The three structures occurring for this system—the sausage, the pizza, and the cluster—are studied separately.

First, note that the CT gives the correct succession of the structures. The volume of the sausage system is smaller than that of a cluster system, which in turn is less than the volume of pizza configurations. On the other hand, the surface area (see the inset) is largest for sausages, then comes the pizza, and finally the cluster configurations. Upon increasing λ_V, both volume and area decrease, as expected, and the conformations become more compressed.

Apparently the CT results give larger values for volume and surface area than the computer simulation. However, the general dependence of the volume coupling looks very similar, especially the limiting behavior for $\lambda_V \to 0$ and for $\lambda_V \to \infty$. The latter even gives the correct value, since the CT becomes exact for zero temperature.

Remember that the CT neglects configurations where particles are located outside their cells. These have larger containers than those taken into account in CT. Hence one might be misled to conclude that CT should give too small $\langle V \rangle$ and $\langle A \rangle$. The fact that both quantities are overestimated is merely due to the construction of the approximate container K^*. This object is a superset of all possible containers where particles are inside cells.

Next, we study the case of $N=13$ particles [Fig. 6(b)] as an example of a system with an intermediate number of particles. In order to apply CT to that system, we have to specify the configurations under examination. This is clear for the sausage, and we choose an exemplary pizza. For the cluster, we pick a regular icosahedron, with an extra particle at its center. We chose this configuration because it was found frequently during simulation runs. However, this structure has some special properties. First, it is not the densest possible cluster for $N=13$. One with smaller volume can be obtained by cutting a spherical region out of a close-packed fcc lattice. Second, in this configuration all particles in the outer shell have enough space to move around freely on the surface of the central sphere. Therefore, the assumption made in CT that all particles are confined to separate regions might be critical. The results are plotted in Fig. 6(b), which shows the same quantities as before. For the surface area (inset), we now see very good agreement between simulation and CT results. At first sight, the plot of the container volume shows the same tendencies as for $N=4$. The general behavior is correct, but the CT overestimates the volume.
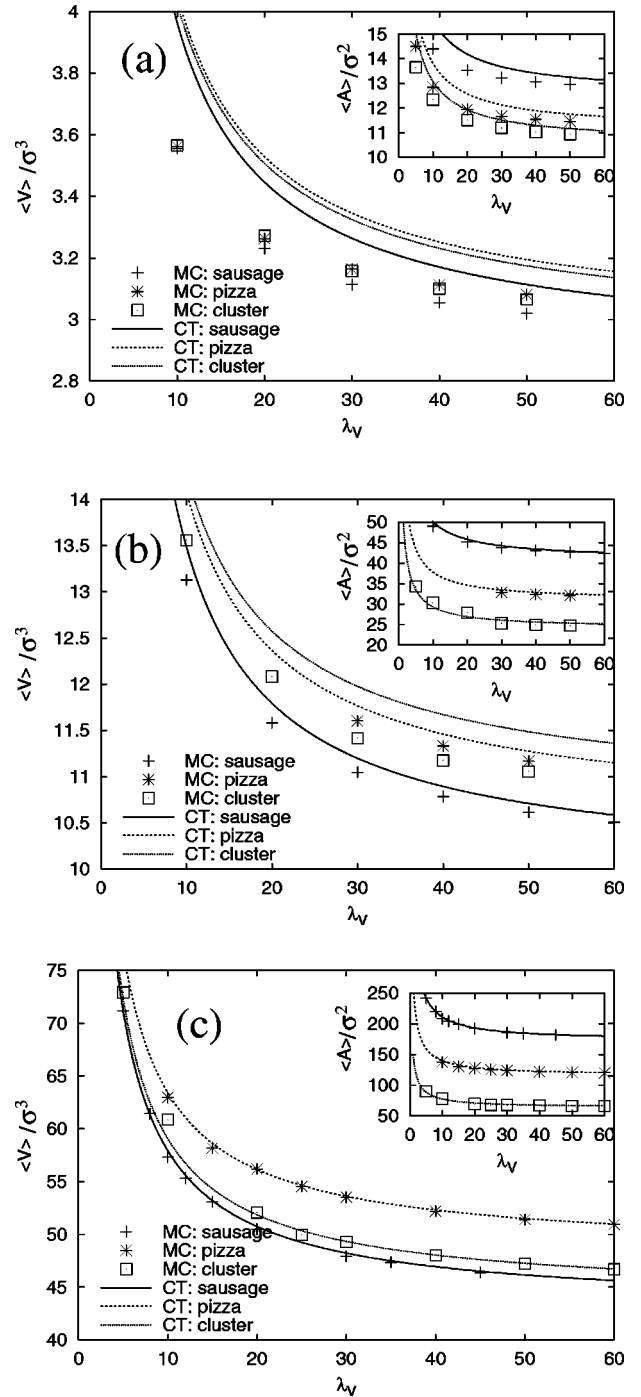

FIG. 6. Average volume $\langle V \rangle / \sigma^3$ as a function of volume coupling λ_V from simulation (MC) and cell theory (CT). Shown are the values for sausage, pizza, and cluster configurations. The inset shows the average surface area $\langle A \rangle / \sigma^2$ as a function of λ_V for different particle numbers N. (a) $N=4$; (b) $N=13$; (c) $N=55$.

Here the discrepancy is smaller for sausage and pizza structures. Note, however, that the order of the lines is shifted. Here, the CT gives a higher volume for the cluster than for the pizza configurations. We attribute this failure of CT to the special properties of the icosahedron cluster. The particles do not stay in the cells as assumed in the theory, so it cannot give accurate results.
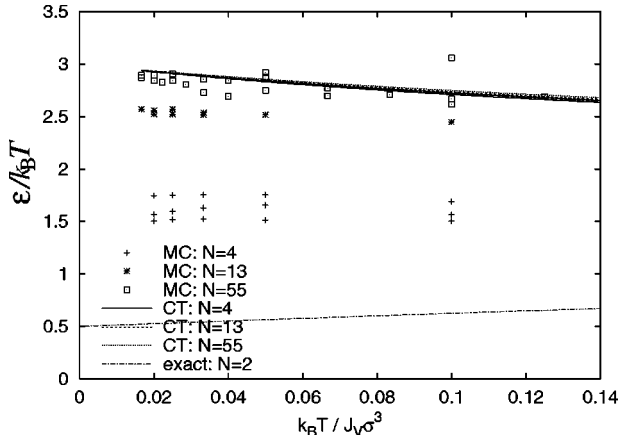
FIG. 7. Excess (over ground-state) internal energy ϵ (in units of $k_B T$) per particle as a function of temperature. Shown are the simulation (MC) and cell theory (CT) results for sausage, pizza, and cluster configurations for $N = 4, 13, 55$, together with the exact solution for $N = 2$.
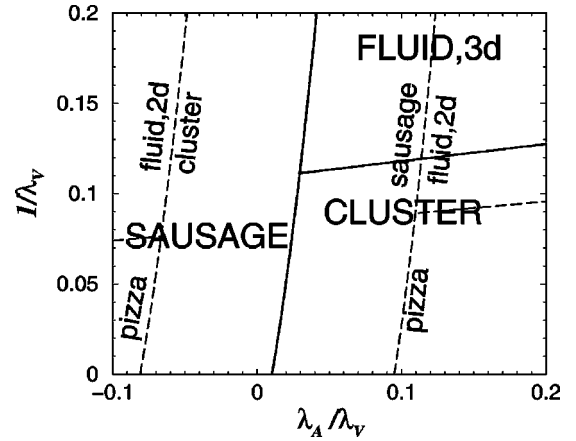

FIG. 8. Phase diagram for $N = 55$ confined colloids as a function of the ratio between surface and volume coupling, λ_A / λ_V, and inverse volume coupling $1/\lambda_V$. The solid lines separates stable states (uppercase), the dashed lines separate metastable states (lowercase).

For $N = 55$, we cut out a portion of a hexagonal lattice for a representative pizza configuration. Similarly, we construct a cluster of 55 particles by cutting a spherical portion out of an fcc lattice. In Fig. 6(c), results for average volume and surface area are given. Excellent agreement between theory and simulation is found.

Summarizing these results, we find that CT gives the correct behavior of equilibrium properties of the system. It overestimates the mean volume, but this deviation decreases for larger particle numbers. One exception is the icosahedral structure of the $N = 13$ cluster, which causes a special difficulty due to its geometric properties. As the complete packing problem is a complicated one, we expect that more such exceptional cases can be found by varying N. The fact that CT predicts more accurate results for higher particle numbers can be attributed to the relative decrease of the number particles at the boundary. We believe that the high accuracy for $N = 55$ is preserved when N is increased, even far beyond this value. Remember that in the thermodynamical limit, $N \rightarrow \infty$, CT gives a fair description of the bulk crystal [30,31].

We next consider the question of how much each particle contributes to the total internal energy of the system. If the temperature of the system is increased, the container swells, which results in an excess volume compared to its close-packed volume V_{CP} at zero temperature. This increase in container volume leads to a gain in internal energy per particle, which is given as $\epsilon = J_V(\langle V \rangle - V_{CP})/N$. We plot $\epsilon/k_B T$ in Fig. 7 as a function of scaled temperature. Shown are the results from both simulation and CT for $N = 4, 13, 55$ and for sausage, pizza, and cluster configurations. For comparison, the exact solution for $N = 2$ is also shown. The dependence on the scaled temperature $k_B T / J_v \sigma^3$ is weak. The simulation data show a global shift to higher values as N increases, but only a minor dependence on the conformation. CT fails to describe the behavior for small N, but gives the correct results for $N = 55$.

C. Transitions between different shapes

As the CT permits direct access to the free energy, we can calculate a ''phase diagram'' as a function of the coupling

parameters. We define a stable phase as the structure with the smallest free energy, which has the largest statistical weight. However, as the system is not in the thermodynamic limit, the probability for conformation with larger free energy does not vanish. We find that either the sausage or the cluster is most stable, see Fig. 8. The horizontal axis is the ratio between volume and surface coupling, λ_A / λ_V. The vertical axis is the inverse volume coupling $1/\lambda_V$. Remember that $\lambda_V = J_v \sigma^3 / k_B T$, so that $1/\lambda_V$ can be regarded as a temperature, whereas $\lambda_A / \lambda_V = J_A / (J_V \sigma)$ is independent of temperature. For fixed temperature, we follow a horizontal path in the phase diagram by changing the ratio λ_A / λ_V. The container is in either the sausage or the cluster state. For small λ_A / λ_V the sausage is stable, as this is the most dense structure in terms of occupied volume. Increasing λ_A / λ_V leads to stabilization of the cluster, because this more compact object possesses smaller surface area. The location of the crossover (phase boundary) shifts towards large λ_A / λ_V upon increasing temperature. If λ_A / λ_V is sufficiently large, the cluster is the ground state at $T = 0$ and remains stable for small T. Increasing T leads to a transition to the sausage. In both regions of the phase diagram, there are two metastable states. The free energies of those can also be compared in order to conclude which of both is relatively more stable. The resulting boundaries show that close to the sausage-cluster transition, the pizza is least stable, but at extreme λ_A / λ_V it will be more stable than the other metastable state. However, the pizza structure never has the lowest free energy of all three conformations. For high T, it is expected that the container does not exert enough pressure on the particles to confine them to well-defined lattice sites, and melting will occur. In infinite bulk systems, this phenomenon depends crucially on dimensionality. It is absent (for short-ranged interactions) in 1D, and the location and even the scenario are different in 2D and 3D. In order to estimate where melting occurs in the present system, we use the following rough criterion. The particles will be fluidlike if the nearest-neighbor distance exceeds the value in the corresponding bulk system, which is

$d = 1.086$ in 2D and $d = 1.11$ in 3D. Within CT, the nearest-neighbor distance is directly accessible and the corresponding state point can be obtained. The fluid regions obtained in this way are indicated in Fig. 8. As expected, the 2D and 3D fluid appear for large $1/\lambda_V$ (large temperature).

VI. CONCLUSIONS

We have investigated a system of spherical particles confined within a fluctuating container. Our model is a hybrid of colloidal cluster physics and membrane theory and couples the degrees of freedom of the particles and the membrane resulting in new vesicle shapes as rodlike, platelike, and spherelike forms. The container may be physically realized by a membrane that constitutes a vesicle or by an oil droplet in an emulsion. We allow this object to change its shape, and take into account an external pressure and a surface tension towards the surrounding. Our theoretical model uses a description of the droplet shape on a coarse-grained level based on integral geometrical methods. The particles are modeled as a finite number of hard spheres, ranging from 2 to 55.

For this system, we have demonstrated that a zoo of different particle conformations arises. These fall into different classes, namely three-dimensional (3D), planar (2D), and linear (1D) ones, called clusters, pizzas, and sausages, respectively.

The breaking of rotational symmetry is especially striking, as *a priori* the model does not contain any anisotropic interactions. The driving force of these transitions is merely the highly nontrivial close-packed structure of a finite number of spheres. Here, this purely geometric packing problem is cast into a physical one through the consideration of the entropy of the system. It allows us to investigate the behavior away from close-packing as a function of container volume and surface area.

As an outlook, we comment on possible future work.

Within the current model, there are still many open questions. One could investigate the effect of nonvanishing coupling to the integral mean curvature, i.e., $\lambda_M \neq 0$. This might be a way to stabilize pizza structures, which were found to be only metastable in the current investigation. Furthermore, one could consider insertion and escape of particle, i.e., use the grand-canonical ensemble with respect to N. A straightforward generalization is towards a collection of more than one container. The coupling to the Euler characteristic λ_χ plays the role of a chemical potential of the containers. As the simplest model, one could neglect the steric interaction between the container hulls themselves, and only take into account the hard cores of particles of different containers.

Furthermore, it would be interesting to model the container in more detail. Using Helfrich's Hamiltonian and a microscopic model for the membrane constitutes an interesting as well as demanding perspective. It is in principle possible to find a suitable experimental setup in which one is able to observe the predicted transitions. Then one could also investigate the dynamics of the rare events of the conformational changes, which is also interesting from a more theoretical point of view. We also mention the interesting problem of crystallization of many of these flexible objects filled with colloidal spheres. Furthermore, it would be interesting to investigate tangent hard spheres inside a flexible container in order to study a polymer chain confined to a vesicle. In this case, one would expect that the ''pizza'' conformation is much less stable. Whether our geometric approach can be used to study hydrophobicity[34] constitutes a further interesting point.

ACKNOWLEDGMENTS

---

[1] P. K. Doye and D. J. Wales, Science **271**, 484 (1996).

[2] K. M. Ho, A. A. Shvartsburg, B. C. Pan, Z. Y. Lu, C. Z. Wang, J. G. Wacker, J. L. Fye, and M. F. Jarrold, Nature (London) **392**, 582 (1998).

[3] D. J. Wales and P. K. Doye, J. Phys. Chem. A **101**, 5111 (1997).

[4] J. M. Wills, Mathematika **43**, 229 (1996).

[5] T. C. Hales, Discrete Comput. Geom. **17**, 1 (1997); **18**, 135 (1997).

[6] A. Maritan, C. Micheletti, A. Trovato, and J. R. Banavar, Nature (London) **406**, 287 (2000).

[7] J. M. Wills, in *Spatial Statistics and Statistical Physics*, edited by K. Mecke and D. Stoyan, Lecture Notes in Physics Vol. 332 (Springer, Berlin, 2000).

[8] H. Löwen, Phys. Rep. **237**, 249 (1994).

[9] H. Löwen, in *Spatial Statistics and Statistical Physics*, edited by K. R. Mecke and D. Stoyan, Lecture Notes in Physics Vol. 554 (Springer, Berlin, 2000).

[10] M. Schmidt and H. Löwen, Phys. Rev. Lett. **76**, 4552 (1996).

[11] M. Schmidt and H. Löwen, Phys. Rev. E **55**, 7228 (1997).

[12] A. K. Macpherson, Y. P. Carignan, and T. Vladimiroff, J. Chem. Phys. **87**, 1768 (1987).

[13] A. González, J. A. White, F. L. Román, S. Velasco, and R. Evans, Phys. Rev. Lett. **79**, 2466 (1997).

[14] Z. T. Nemeth and H. Löwen, J. Phys.: Condens. Matter **10**, 6189 (1998).

[15] F. L. Roman, M. Schmidt, and H. Löwen, Phys. Rev. E **61**, 5445 (2000).

[16] U. Seifert, Adv. Phys. **46**, 13 (1997).

[17] R. Lipowsky, Encyclopedia Appl. Phys. **23**, 199 (1998).

[18] G. Gompper and D. M. Kroll, Curr. Opin. Colloid Interface Sci. **2**, 373 (1997).

[19] A. R. Bausch, F. Ziemann, A. A. Boulbitch, K. Jacobson, and E. Sackmann, Biophys. J. **75**, 2038 (1998).

[20] M. Ficheux, L. Bonakdar, F. Leal-Calderon, and J. Bibette, Langmuir **14**, 2702 (1998).

[21] R. Bar-Ziv, T. Frisch, and E. Moses, Phys. Rev. Lett. **75**, 3481 (1995).

[22] A. D. Dinsmore, D. T. Wong, P. Nelson, and A. G. Yodh, Phys. Rev. Lett. **80**, 409 (1998).

[23] R. Lipowsky and H. Döbereiner, Europhys. Lett. **43**, 219 (1998).

[24] K. R. Mecke, in *Spatial Statistics and Statistical Physics*, edited by K. R. Mecke and D. Stoyan, Lecture Notes in Physics Vol. 111 (Springer, Berlin, 2000).

[25] C. N. Likos, K. R. Mecke, and H. Wagner, J. Chem. Phys. **102**, 9350 (1995).

[26] K. R. Mecke, J. Phys.: Condens. Matter **8**, 9663 (1996).

[27] K. R. Mecke, Int. J. Mod. Phys. B **12**, 861 (1998).

[28] C. B. Barber, D. P. Dobkin, and H. Huhdanpaa, ACM Trans. Math. Softw. **22**, 469 (1996).

[29] W. Helfrich, Z. Naturforsch. C **28c**, 693 (1973).

[30] J. G. Kirkwood, J. Chem. Phys. **18**, 380 (1950).

[31] W. W. Wood, J. Chem. Phys. **20**, 1334 (1952).

[32] M. Heni and H. Löwen, Phys. Rev. E **60**, 7057 (1999).

[33] Different cell shapes primarily generate a constant factor in the partition sum, which does not affect expectation values.

[34] K. Lum, D. Chandler, J. D. Weeks, J. Phys. Chem. B **103**, 4570 (1999).